Dielectric Relaxation Spectroscopy of Hydrated and Dehydrated Silk Fibroin Cast from Aqueous Solution

ARTICLE *in* BIOMACROMOLECULES · OCTOBER 2010

Impact Factor: 5.75 · DOI: 10.1021/bm1008316 · Source: PubMed

4 AUTHORS, INCLUDING:

Xiao Hu
Rowan University
79 PUBLICATIONS **2,873** CITATIONS
SEE PROFILE

Peggy Cebe
Tufts University
248 PUBLICATIONS **4,658** CITATIONS
SEE PROFILE

Dielectric Relaxation Spectroscopy of Hydrated and Dehydrated Silk Fibroin Cast from Aqueous Solution

Lei Yu,[†] Xiao Hu,[‡] David Kaplan,[‡] and Peggy Cebe*[,†]

Department of Physics and Astronomy and Biomedical Engineering Department, Tufts University, Medford, Massachusetts 02155

Received July 20, 2010; Revised Manuscript Received August 28, 2010

The dynamics of silk protein in the presence and absence of water has been investigated by dielectric relaxation spectroscopy (DRS). The silk fibroin film cast from its water solution contains 4−7 wt % bound water molecules, which can be removed by dehydration at 165 °C. Temperature and frequency scans were performed on the hydrated and dehydrated samples over the temperature range from −100 to 280 °C, and frequency range from 20 to 1 MHz. Temperature scans of hydrated samples show three relaxation peaks, including β- and α-relaxations, related to bound water and to the glass transition. A new third peak, denoted as α', was seen in hydrated sample at around 60 °C, and its intensity increases with decreasing frequency. On the other hand, in the completely dehydrated sample, the β- and α'-relaxation peaks both disappeared, which reveals their origin from bound water molecules. The α' process is attributed to the removal of bound water, after which the glass transition of dehydrated silk appears at higher temperature as the α process. Real-time DRS has also been performed to monitor isothermal crystallization. Both the dielectric constant, ε', and conductivity, σ, decrease gradually as the crystallization proceeds. Analysis of dielectric modulus shows that both conductivity and the α-relaxation are observed at the beginning of crystallization. As the crystal grows, the α-relaxation starts gradually to diminish both in strength and in rate. Before crystallization, α-helices and random coils with dipole moments are the major components in silk fibroin. During crystallization, α-helices can be transformed into antiparallel β-sheets, which possess no dipole moment, causing the decreasing trend in the dielectric parameters as crystallization proceeds.

1. Introduction

Bombyx mori silk has been used in the textile industry for thousands of years due to its special luster and mechanical properties. Silks from silkworms can be easily obtained from the naturally made silk cocoon and, therefore, have been widely used to explain the processing mechanisms of all silks and to exploit their properties for use as natural polymers and biomaterials.[1−10] Silks are unique, combining high extensibility and high tensile strength.[11] On a strength-to-weight basis, the toughness of some silk species is higher than that of Kevlar fibers.[3,5] In addition to their impressive mechanical properties, silks have many advantages such as environmental stability, biocompatibility, controlled biodegradability, and morphologic flexibility.[1−11] Silk can be cast from its water solution into thin film, which is similar to conventional thermoplastic film[12−14] or electrospun into nanofibers with high-voltage electrospinning technique[15,16] that can be used as biocompatible scaffold in tissue engineering. Thus, silks represent a unique family of structural proteins that are not only useful within the traditional polymer industry, but also offer a wide range of biocompatible properties in the newly risen biomedical industry.

Protein−water interaction in silk fibroin plays an interesting and important role in changing its physical properties, such as the glass transition temperature. Bound water molecules can act as a plasticizer[13] and become incorporated into the silk fibroin structure and increase its flexibility and extensibility. By decreasing the inter- and intramolecular friction and effective barrier height for conformational change in the silk fibroin, the bound water can induce a new "glass transition" with lower T_g, which is around 80 °C, compared to 178 °C in the fully dehydrated sample.[13] Upon heating the hydrated silk fibroin to a higher temperature, thermal energy will be increased and some bound water molecules will be liberated into free water molecules. Below the glass transition temperature, as the interaction between bound water and polymer molecules is broken, a structure transformation of the silk fibroin will be induced, which was described in our previous work[13] as a "precursor" structure forming prior to crystallization.

As temperature increases above the glass transition temperature of fully dried silk, the crystallization of β-sheet structure occurs. We showed that the crystallization process of silk fibroin follows a mechanism similar to conventional cold crystallized polymer.[13] A precursor structure was proposed to exist after the removal of bound water molecules when temperature increases above 80 °C, which promotes the crystallization of β-sheet structure when the temperature further increases above the glass transition temperature at 178 °C. Crystallizable protein structures are analogous to the block copolymer structures. Silk fibroin has been shown to contain many crystallizable amino acid blocks or domains as well as the uncrystallizable domains. Our recent study[14] presented a model to explain the isothermal crystallization process of silk fibroin. During isothermal crystallization, strong hydrogen bonds are formed leading to the formation of a β-sheet structure in the crystallizable domains, which are phase-separated from the noncrystallizable parts of the silk fibroin.

In our previous work, we utilized X-ray diffactometry, Fourier transform infrared spectroscopy (FTIR), and differential scanning calorimetry (DSC) to investigate the crystal structure, infrared vibrational bands, and heat capacity of silk fibroin.

* To whom correspondence should be addressed. Tel.: 617-627-3365. E-mail: peggy.cebe@tufts.edu.
[†] Department of Physics and Astronomy.
[‡] Biomedical Engineering Department.

10.1021/bm1008316
Published on Web 09/21/2010

Because the peptide and hydrogen bonds, which are the essential links in protein, possess a net dipole moment, it is feasible to apply dielectric relaxation spectroscopy (DRS) to monitor their structure variation during the dehydration and crystallization processes. DRS has been extensively used in investigating biopolymers, such as proteins and DNAs.[17,18] Mijovic et al.[18] investigated the interactions between water and three globular proteins: *Candida antarctica* Lipase B (CaLB), bovine serum albumin (BSA), and lysozyme (Lys). Three dielectric dispersions were observed in each hydrated protein and their molecular origins were discussed. The same group also investigated the dynamics of aqueous solutions of deoxyribonucleic acid (DNA).[17] Two dielectric relaxation peaks below 0 °C were attributed to the bound water around DNA molecules and to pure ice. In the higher temperature range, another relaxation peak was observed and its origin is the migration of counterions along the DNA surface.

Previous papers discussed the dielectric properties of silk fibroin.[19,20] Magoshi et al.[19] performed temperature scans at several frequencies and two dielectric relaxation processes were found, which are located at about −40 and 175 °C. The peak in the low temperature range, denoted as β, was claimed to be due to the water-coupled local mode motion in the random coil conformation. The β-relaxation showed Arrhenius characteristic when the log(frequency) was plotted versus reciprocal temperature. Another relaxation peak in the high temperature range was also found, and this peak could not, at that time, be assigned to any mechanism, but it disappeared in the dehydrated silk. More recently, a comparative study of the dielectric and mechanical relaxation of silk fibroin was performed by Um et al.[20] A dielectric relaxation study exhibited a higher sensitivity in the lower temperature range, revealing the γ-relaxation. Dynamic mechanical analysis is better suited to investigate relaxation behaviors in the higher temperature range, including α- and α_c-relaxations, according to these authors.[20]

The two references mentioned above[19,20] investigated the temperature dependence of dielectric properties during heating. In our present study, to shed more light on mechanisms of silk fibroin relaxations, we utilized the DRS technique to investigate the electrical properties of hydrated and dehydrated silk fibroin in both frequency and temperature range and also, for the first time, its isothermal crystallization process. The hydrated sample was cast from silk water solution with 4−7 wt % bound water molecules inside. The bound water can be eliminated when holding the sample at any temperature higher than 100 °C for 30 min. The dehydrated sample was also studied by DRS to make a comparison with the hydrated sample. The bound water molecules are believed to be responsible for two relaxations occurring in the protein. The conformational transition from α-helix to β-sheet structure is applied to explain the phenomena observed in the DRS data of the isothermal crystallization process.

2. Experimental Section

2.1. Material Preparation. The silk fibroin preparation process has been reported.[21−26] Briefly, *B. mori* silkworm cocoons were first boiled in a Na_2CO_3 solution to extract the sericin, the efficacy of which has been verified previously.[26] The remaining silk fibroin fiber was dissolved in LiBr solution at 60 °C and then dialyzed against distilled water multiple times to remove the LiBr. After centrifugation and filtration, the final 2 wt % silk fibroin aqueous solution was cast onto polystyrene dishes to generate the uncrystalline silk fibroin films (around 10−20 μm thick). The samples were gold-coated by thermal evaporation before the dielectric measurement. To obtain dehydrated samples, we held the sample isothermally at 165 °C for 30 min. Thermal gravimetric analysis shows that this is sufficient to remove bound water and FTIR analysis shows that there are no β-sheet crystals formed in the dehydrated sample.

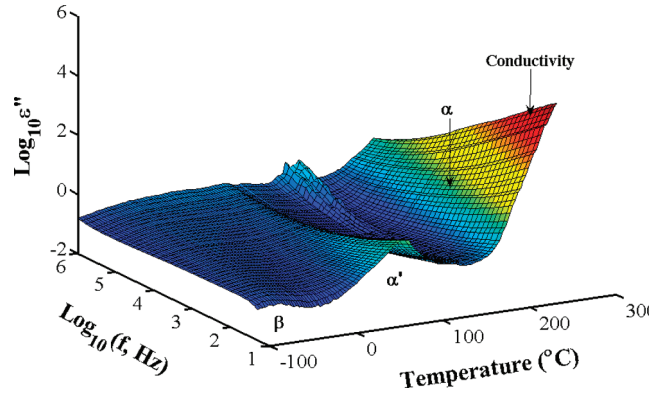

Figure 1. Three-dimensional DRS spectrum of dielectric loss with frequency and temperature as variables for hydrated silk fibroin protein. Several relaxation processes are marked. The α-relaxation peak is masked by the conductivity relaxation at high temperature and low frequency. Around 100 °C dielectric properties show erratic behavior in the high frequency region due to removal of bound water during heating.

2.2. Analysis Methods. An ARES system from TA Instruments coupled with an Agilent LCR Meter 4284A were utilized to measure the dielectric properties of the silk fibroin thin film sample. For temperature scans, the sample was placed in the ARES between two stainless steel electrodes with diameter 25 mm and temperature ramp using 2 or 4 °C/min was performed while taking measurements with 10 different preset frequencies. For frequency scans, the thin film sample was put in the ARES for temperature control and isothermally measured with 40 select frequencies in the range from 20 Hz to 1 MHz. The temperature was controlled by the ARES with liquid nitrogen at low temperature and dry compressed air at high temperatures.

3. Results and Discussion

3.1. Temperature-Dependent Properties. Figure 1 shows the 3D DRS spectrum of hydrated silk fibroin with a frequency range from 20 Hz to 1 MHz and a temperature range from −100 to 245 °C. Several relaxation peaks are marked, which will be discussed in more detail. During heating of hydrated sample, bound water is released when the temperature is close to or above 100 °C. This leads to a spurious signature in the dielectric spectrum seen in Figure 1 at high frequencies. Figure 2a,b shows the DRS temperature scan of hydrated and dehydrated silk, respectively, while heating from −100 to 280 °C at 2 °C/min. In the low temperature range, −100 to 20 °C, one relaxation peak, denoted as β, is detected and the peak position shifts to higher temperature as frequency increases, shown in Figure 2a. The disappearance of the β-relaxation in the dehydrated sample, shown in Figure 2b, suggests that the relaxation is related to bound water. The second peak, denoted as α′, appears at around 60 °C, shown in Figure 2c. Interestingly, the position of this peak almost stays at the same temperature when frequency increases but the intensity decreases quickly with increasing frequency. In the dehydrated sample, this peak totally disappears, as shown in Figure 2d. Nogales et al.[27] found a similar dielectric relaxation peak in Chitosan located at around 80 °C. The origin of that ε'' peak was associated with desorption of bound water. In our previous work,[28] thermogravimetric analysis (TGA) of silk fibroin also showed that bound water was removed gradually during heating over the temperature range from around 32−150 °C, which overlaps with the effective temperature region of the α′ peak. This

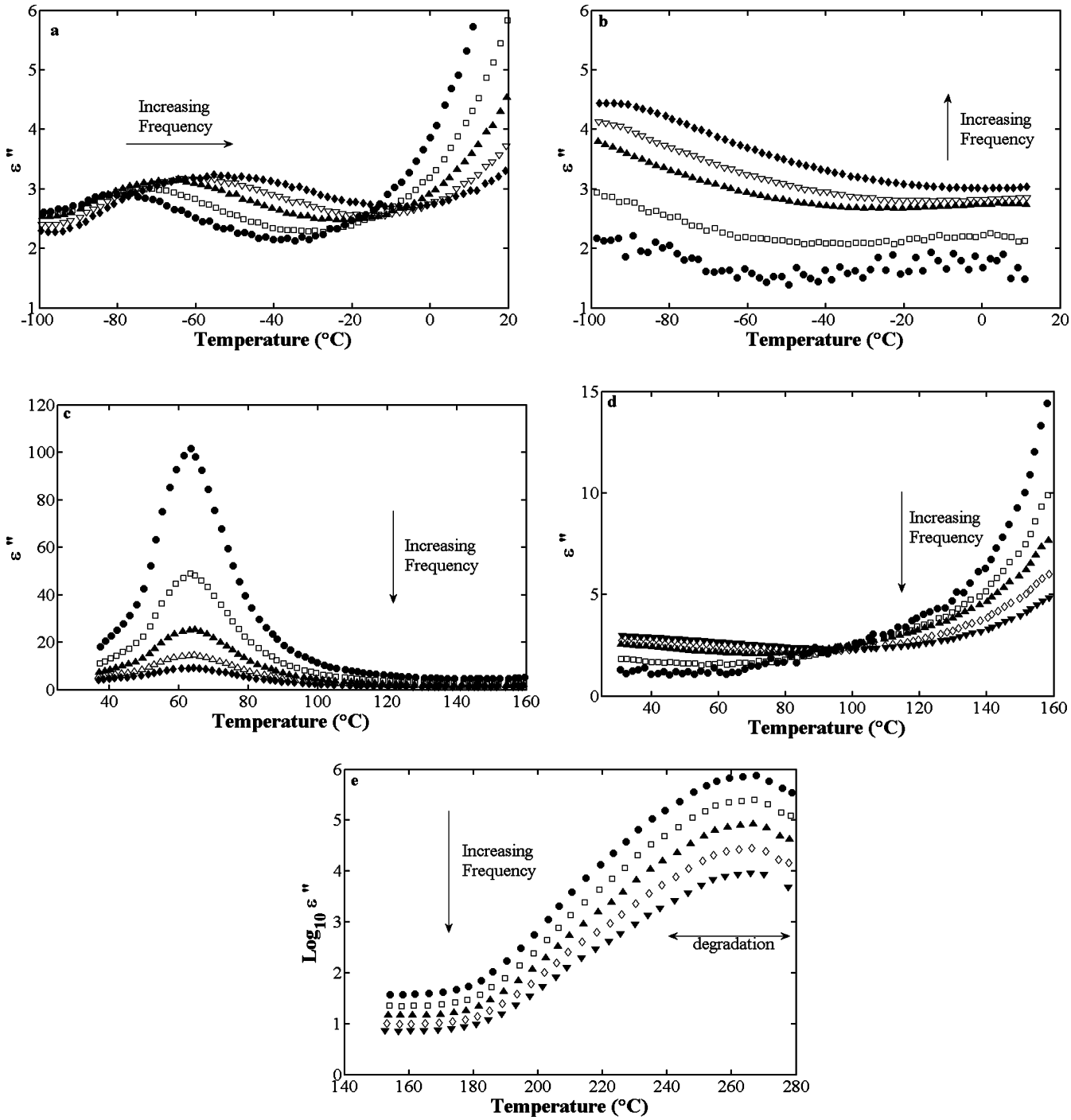

Figure 2. Dielectric loss vs temperature of silk fibroin protein below room temperature for (a) hydrated sample and (b) dehydrated sample; from room temperature to 160 °C for (c) hydrated sample and (d) dehydrated sample; from 150 to 280 °C for (e) dehydrated sample. Frequencies chosen are 46 (●), 139 (□), 422 (▲), 1277 (♦), and 3906 Hz (▽). Heating rate is 2 °C/min in (a−d) and 4 °C/min in (e).

may indicate that the α′-relaxation peak is related to bound water removal in the silk fibroin sample, as it is in Chitosan.

The α peak of dehydrated silk always occurs above T_g = 178 °C and the bound water molecules are already eliminated at this temperature, so no comparison can be made between hydrated and dehydrated samples. Figure 2e shows the higher temperature range from 150 to 280 °C. The high temperature behavior is due to the degradation of silk, which occurs above 225 °C and the α-relaxation is believed to be masked at high temperature by DC conductivity.

3.2. Frequency-Dependent Properties. To obtain more information on the dynamic electrical response of silk fibroin, we measured the dielectric spectrum in the frequency domain at selected temperatures. A β-relaxation peak was found in the temperature range from −60 to 0 °C for hydrated sample as a function of frequency (20 Hz–1 MHz). The peak was broad and shifted to higher frequency with increasing temperature. From Figure 3a, the peak was visible until −15 °C, where the high frequency end starts to increase steeply; at 0 °C, only a shoulder for the peak can be observed. The Arrhenius plot shown in Figure 3b was used to describe the relationship between f_{max} versus reciprocal of temperature. The activation energy is found to be 27 kJ/mol, which is less than the value reported by Magoshi (46 kJ/mol).[19]

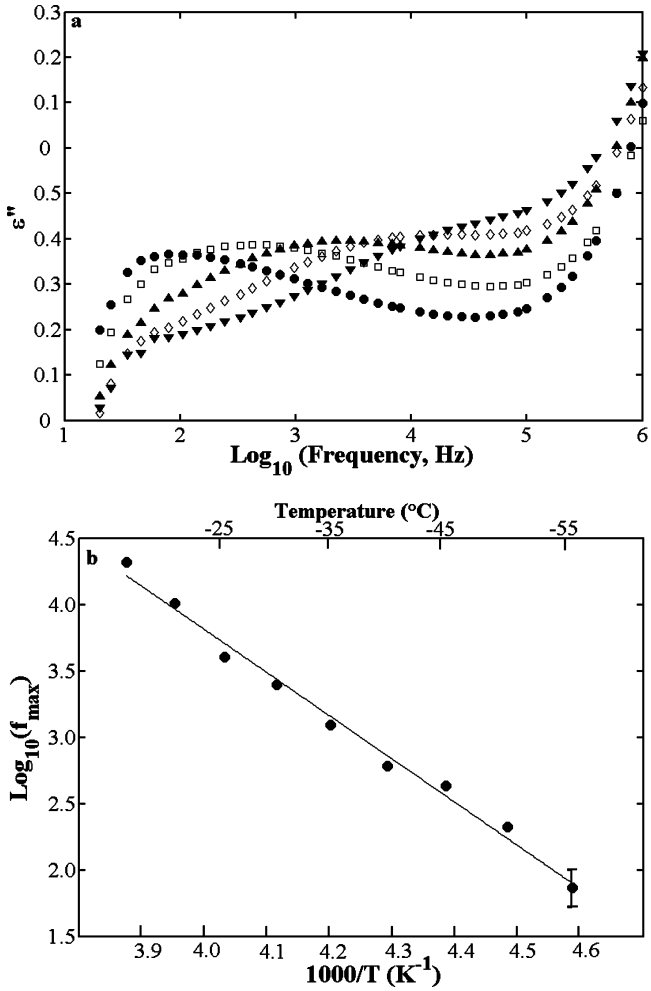

Figure 3. β-Relaxation from −60 to 0 °C for hydrated silk fibroin protein: (a) ε'' vs $\log_{10}f$; −60 °C (●), −45 °C (□), −30 °C (▲), −15 °C (◇), 0 °C (▼). (b) Arrhenius plot of the β-relaxation for silk fibroin protein. The right-most point has error bar indicated. All other data have error bars smaller than the symbol width.

The hydrated sample was then held at 165 °C for 30 min to become fully dried and then the measurement was taken again in the low temperature range. We found the β-relaxation peak disappeared completely. The ε'' exhibited almost a flat line (data not shown) compared to the peak before dehydration, showing that the β-relaxation peak is only related to the interaction between the bound water molecules and the silk polymer chains.

Nylon-6 has been investigated thoroughly by DRS.[29,30] The dipolar structure of Nylon-6 is similar to silk protein, having carbonyl and amine groups linked with an amide bond except that silk and nylon possess different chemical groups as side chains on the polymer chain backbone. In Nylon-6, there are two dielectric relaxations denoted as γ and β found at low temperature. The tightly bound water molecules that create double hydrogen bonds between neighboring C═O groups were claimed to be responsible for the γ-relaxation, and the β-relaxation originated from the interaction between water and C═O groups. Our calculated activation energy for the β-relaxation of silk is 27 kJ/mol, which is between the typical value of 21 kJ/mol for the hydrogen bond in O−H···O and 29 kJ/mol in O−H···N. This may indicate that the origin of the β-relaxation in silk is related to the hydrogen bond formed between bound water and the C═O and N−H of the silk amino acid groups.

The glass transition can be seen occurring at temperature higher than the DSC-determined thermal T_g (178 °C).[13] The

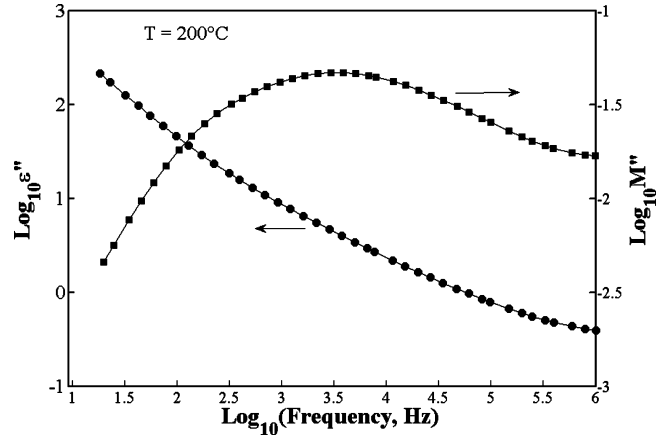

Figure 4. Dielectric loss permittivity, ε'' (●) and modulus M'' (■), at $T = 200$ °C for silk fibroin protein.

model function of Havriliak−Negami (H-N)[31] is commonly used to analyze the dielectric measurement quantitatively:

$$\varepsilon^*(\omega) = \varepsilon'(\omega) - i\varepsilon''(\omega) = \varepsilon_\infty + \frac{\Delta\varepsilon}{(1 + (i\omega\tau)^\beta)^\lambda} - i\frac{\sigma_0}{\omega^s\varepsilon_0} \quad (1)$$

In the H-N equation, $\varepsilon^*(\omega)$ is the complex dielectric permittivity while ε' and ε'' are the dielectric permittivity and loss, respectively; $\omega = 2\pi f$ is the radian electric field oscillation frequency; ε_s and ε_∞ are the high and low frequency limits of the dielectric constant; $\Delta\varepsilon$ is the relaxation strength defined as $\Delta\varepsilon = \varepsilon_s - \varepsilon_\infty$; τ is the relaxation time, which is the reciprocal of the radian frequency of maximal loss ω_{max}; and β and γ ($0 < \beta \le 1$, $0 < \beta\gamma \le 1$) are the shape parameters of the relaxation spectra. In eq 1, the added term $-i[\sigma_0/(\omega^s\delta_0)]$ stands for the conduction effects, where σ_0 is related to the dc conductivity of the sample and ε_0 is the dielectric permittivity of vacuum. The parameter $s = 1$ for ohmic conductivity and $s < 1$ for nonohmic effects in the conductivity.[32,33] However, due to the appearance of DC conductivity effects at low frequency and high temperature, the α-relaxation peak can be masked. Therefore, dielectric modulus M^* formalism is often used to reveal more information from the dielectric permittivity spectra. M^* is defined as[33]

$$M^*(\omega) = \frac{1}{\varepsilon^*(\omega)} = M'(\omega) + iM''(\omega) \quad (2a)$$

$$M'(\omega) = \frac{\varepsilon'(\omega)}{[\varepsilon'(\omega)]^2 + [\varepsilon''(\omega)]^2}, \qquad M''(\omega) = \frac{\varepsilon''(\omega)}{[\varepsilon'(\omega)]^2 + [\varepsilon''(\omega)]^2} \quad (2b)$$

where M' and M'' are the dielectric modulus permittivity and loss. One advantage brought by M^* formalism is that it can transform the steep increase raised by the DC conductivity in the dielectric permittivity spectra into a relaxation peak so that the underlying process is more easily located and analyzed.[34] Figure 4 shows both ε'' and M″ at $T = 200$ °C at time $t = 0$ min, before crystallization has occurred. ε'' increases with decreasing frequency and no peak can be observed. However, the M″ plot reveals a broad peak, the width and shape of which

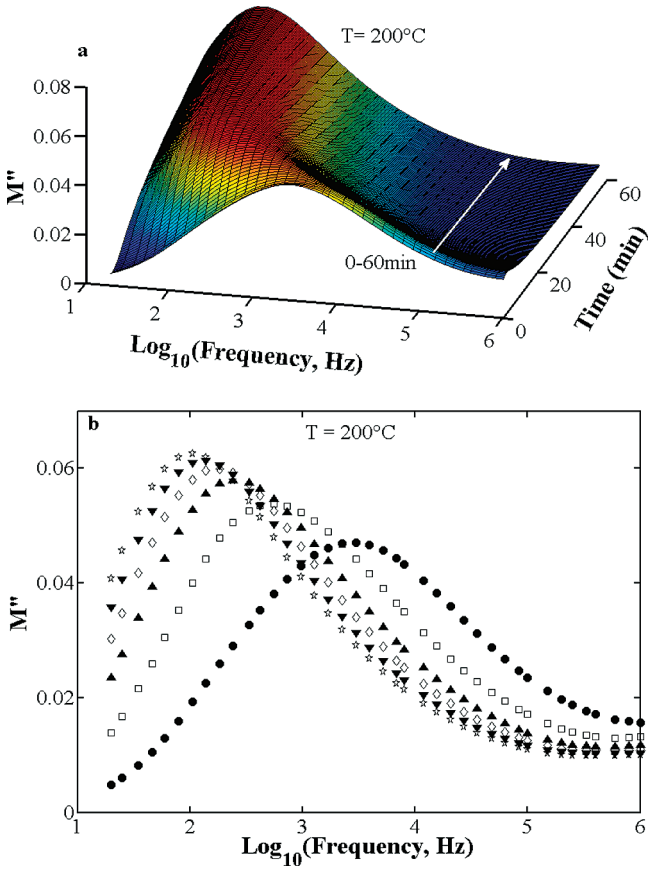

Figure 5. (a) Three dimensional plot of dielectric modulus, M'' vs frequency and time during isothermal crystallization of silk fibroin protein at 200 °C for 1 h; (b) 2D plot of M'' vs frequency during crystallization at 200 °C at times of 0 (●), 10 (□), 20 (▲), 30 (◊), 40 (▼), and 50 min (☆).

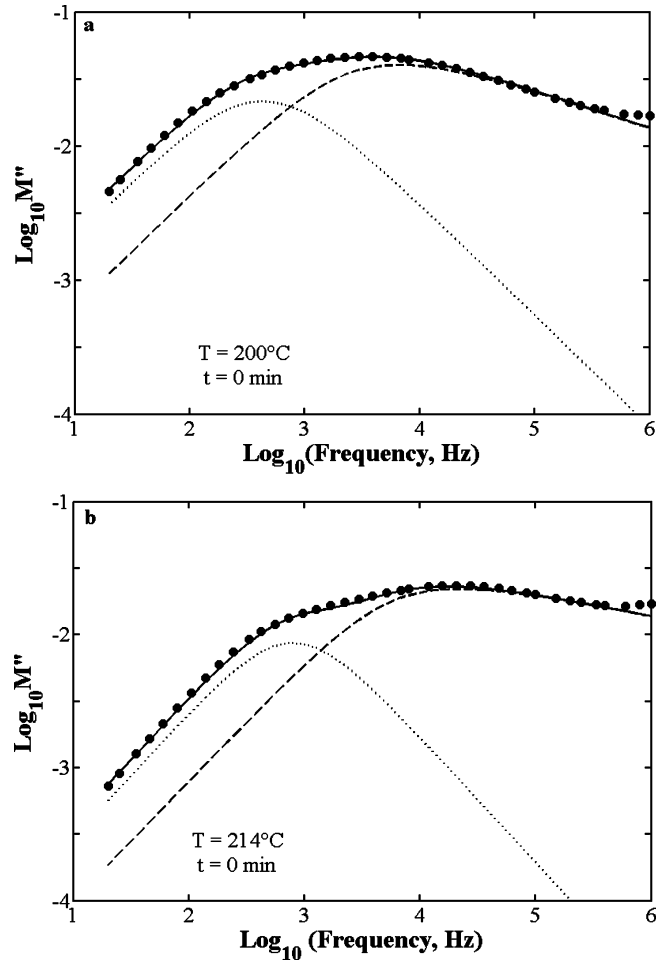

Figure 6. Dielectric loss modulus vs frequency (solid points) for silk fibroin protein at the beginning of isothermal crystallization (time, $t = 0$) at (a) $T_c = 200$ °C and (b) $T_c = 214$ °C. The dashed and dotted lines are two relaxation components fitted from the data points according to eq 3; the solid line represents the total fitted line to the data points.

reveal the multicomponent character of the relaxation process, which will be discussed in detail later in this paper. Readers may consult references[33−37] for additional information about the dielectric modulus.

3.3. Isothermal Crystallization. Because the α-relaxation, which is related to the glass transition, occurs in the similar temperature region with the isothermal crystallization, we use DRS for the first time to investigate the variation of the α-relaxation during the isothermal crystallization of silk fibroin β-sheets. First, we used real-time DRS to monitor the dielectric relaxation behavior of silk fibroin during isothermal crystallization at T_c for a time long enough to guarantee complete crystallization (typically 30 or 60 min). After the crystallization was completed, we remeasured the dielectric relaxation properties at several temperatures below T_c to get more information about the after-crystallization status of the silk fibroin.

Previous work from our group[13] has used real-time FTIR and X-ray techniques to study the isothermal crystallization of silk fibroin film at temperatures above T_g. FTIR spectrum for a sample held at 200 °C for 1 h shows that the intensity of vibrational bands representing α-helices and random coils decreases and β-sheet crystalline bands increase with crystallization time. Wide angle X-ray scattering for a sample crystallized at 215 °C shows several crystal peaks growing from the amorphous halo as crystallization time increases, and they were identified as originating from β-sheet crystals. Both techniques showed the β-sheet crystals can be formed by cold-crystallization when the silk fibroin is held at temperatures above T_g.

Figure 5a shows the 3D plot of the real time dielectric relaxation spectrum of silk fibroin held at 200 °C for 1 h. The dielectric modulus M'' is used here as introduced previously. As the β-sheet crystals grow with crystallization time, the main relaxation peak position, f_{max}, gradually shifts to lower frequency. In the first 10 min, f_{max} decreased by two decades and then decreased much more slowly, which is consistent with our previous results on crystallization kinetics obtained from X-ray, FTIR, and DSC measurements.[12,13]

A 2D plot with crystallization time at temperature $T_c = 200$ °C is shown in Figure 5b. From this plot, an obvious peak shift to lower frequency can be seen, which means the relaxation slows down with time. Detailed dielectric information can be acquired from fitting of the 2D plot with modified Havriliak−Negami functional form:[17]

$$M^*(\omega) = M_s + \frac{\Delta M}{(1 + (i\omega\tau_M)^a)^b} \qquad (3)$$

where $M_s = 1/\varepsilon_s$, ΔM is the dielectric modulus strength, τ_M is characteristic time, and a and b are shape parameters.

The fitting process decomposes the M'' spectra at the beginning of the isothermal crystallization at $T_c = 200$ and 214 °C into two dielectric relaxation processes shown in Figure 6. As time increases, these two processes become overlapped and harder to separate. We suggest that the relaxation at lower

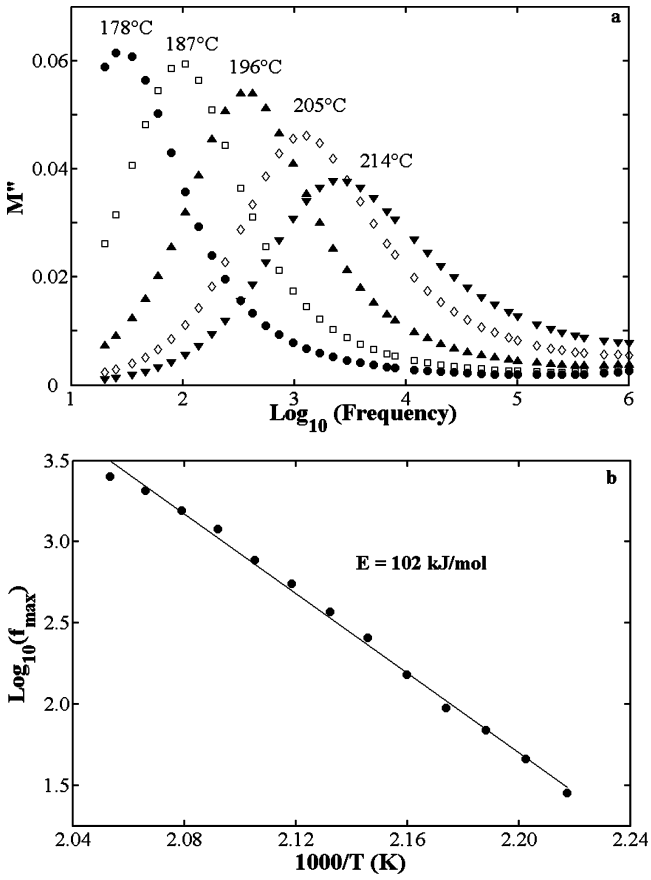

Figure 7. (a) Dielectric loss modulus vs frequency after isothermal crystallization for silk fibroin protein at 214 °C for 30 min, for data taken at the indicated temperatures; (b) Corresponding Arrhenius plot. Error bars have about the same size as the symbols.

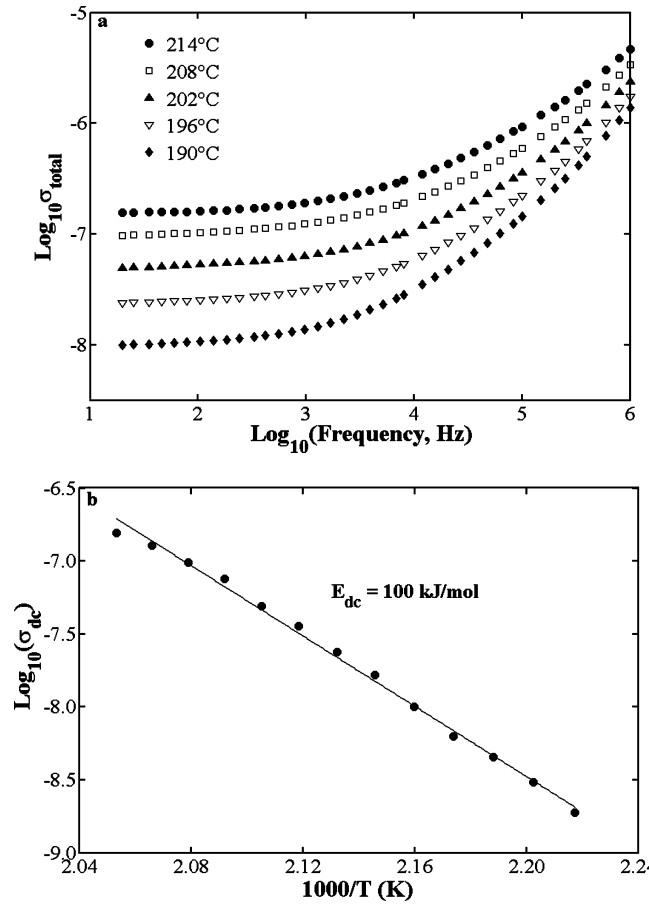

Figure 8. (a) Frequency dependence of DC conductivity of silk fibroin protein at different temperatures below 214 °C. (b) Corresponding DC conductivity vs 1/*T*. The line is the best fit to the data using the Arrhenius relationship. Error bars have about the same size as the symbols.

frequency is the conductivity relaxation raised by the thermal motion of mobile charge carriers at high temperature. The higher frequency process is the α-relaxation, arising from the glass transition within the amorphous regions of silk fibroin.

We measured the dielectric relaxation spectra again after the completion of isothermal crystallization at 214 °C for 30 min to compare them with the spectra at the beginning of the crystallization. The measured M'' relaxation peak is shown in Figure 7a. The maximum frequency position versus the reciprocal of temperature is shown in Figure 7b. However, the raw data points alone provide no selection rule for fitting with the Arrhenius or Vogel−Fulcher−Tammann (VFT) form. Moznine et al.[38] suggests using the following equation to identify which form should be used for the fitting process.

$$\left[\frac{\mathrm{d}\ln\tau}{\mathrm{d}\left(\frac{1}{T}\right)}\right]^{-1/2} = \frac{1}{\sqrt{B}} - \frac{T_0}{\sqrt{B}} \times \frac{1}{T} \tag{4}$$

where the parameters B and T_0 are defined in the VFT equation shown below:

$$\tau = \tau_0 e^{B/(T-T_0)} \tag{5}$$

where τ_0 and B are constants and T_0 is the so-called Vogel temperature. If the plot of derivative of ln τ against the reciprocal of T is independent of $1/T$, then $T_0 = 0$, which means the data can be described with an Arrhenius plot. This is the case for our data, and the Arrhenius plot is shown in Figure 7b, which gives an activation energy of 102 kJ/mol. (We remark parenthetically that the parameter of the dielectric modulus formalism can be related to those from the dielectric permittivity. In particular, $\tau_M = (\varepsilon_\infty/\varepsilon_s)\tau_\varepsilon$ from which $\log \tau_M = \log (\varepsilon_\infty/\varepsilon_s) + \log \tau_\varepsilon$ and, because the $\log (\varepsilon_\infty/\varepsilon_s)$ is a very small number, the $\log \tau_M$ is very close to $\log \tau_\varepsilon$. Therefore, the activation energy determined from modulus data in Figure 7 can be viewed as almost the same as that determined from ε.) To our knowledge, this is the first time that the crystallization of silk fibroin has been analyzed using dielectric techniques.

Mohomed et al.[39] suggest several methods for identifying the conductivity relaxation peak in the dielectric loss modulus M'' spectra of poly(2-hydroxyethyl methacrylate) (PHEMA) sample. One way is to compare the activation energy of the major peak in Figure 7a with that of the DC conductivity in the same temperature range. Figure 8a shows the frequency dependence of total conductivity for several temperatures below 214 °C where conductivity is predominant. The conductivity at 20 Hz, which is the low frequency end for our data, can be approximately regarded as the DC conductivity for each temperature, and its dependence with temperature is expressed in Figure 8b. The activation energy for DC conductivity is calculated as 100 kJ/mol, which is very close to 102 kJ/mol calculated for the major peak in Figure 7a. It was reported that the ionic conductivity peak and DC conductivity possess the same temperature dependence,[36] so the position of the major peak in Figure 7a represents the conductivity relaxation peak position.

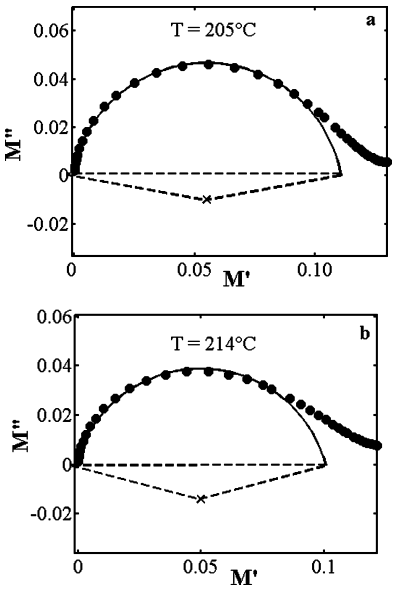

Figure 9. Cole−Cole plot of M' vs M' for silk fibroin protein at (a) 205 and (b) 214 °C, after completion of crystallization at 214 °C. The circles with centers displaced below the axis are the best fits to the data.

According to Mohomed,[39] the Cole−Cole plot of M'' versus M' can also be used to identify the conductivity relaxation. If the plot reveals a true semicircle, it implies the dielectric process follows the Debye model. This is interpreted to mean that the process is a conductivity relaxation, which exhibits a single relaxation time, as suggested previously.[40−42] In our case, the Cole−Cole plots of M'' against M' at 205 and 214 °C, shown in Figure 9a and b, respectively, present symmetrical plots but are not perfect semicircular plots, having centers displaced below the axis. This result means that the major relaxation peak in Figure 7a represents the conductivity relaxation mixed with another viscoelastic relaxation, most likely mixed with the α-process from the glass transition relaxation occurring at higher frequency.

Fitting plots are shown in Figure 10a,b of data taken at 205 and 214 °C, respectively, after crystallization of the silk at 214 °C. The fitting procedure shows that the relaxation peaks in Figure 7a can be described with two relaxation peaks. The relaxation located at lower frequency is attributed to the conductivity relaxation, while the one at higher frequency is believed to be the α-relaxation related to the glass transition. From our previous DSC results,[12] after crystallization at 214 °C silk fibroin still contains 54% of mobile noncrystalline chains (i.e., only 46% has become crystalline β-sheets). For this reason, the α-relaxation, attributed to mobile noncrystalline chains, still exists after crystallization, giving a relaxation peak at higher frequency. The α-relaxation could result from the remaining noncrystalline chains, including (1) crystallizable chain segments that have not become fully crystallized and (2) noncrystallizable parts, including random coils and turns, which also possess dipole moments and are dielectrically active. Comparing Figure 10b with Figure 6b, the α-relaxation after crystallization becomes slower and weaker than that right at the beginning of the crystallization. The formation of crystalline β-sheets consumes the noncrystalline polymer chains in the crystallizable part, weakening the relaxation strength of α-relaxation. The formed crystalline silk fibroin also could cause physical constraints on the α-relaxation of the remaining polymer chains in the noncrystalline part and therefore shift the α-relaxation to lower frequency.

Figure 11a,b shows the change of total conductivity σ_{total} and dielectric permittivity ε', respectively, during isothermal crystallization at $T_c = 200$ °C. The time difference between every two

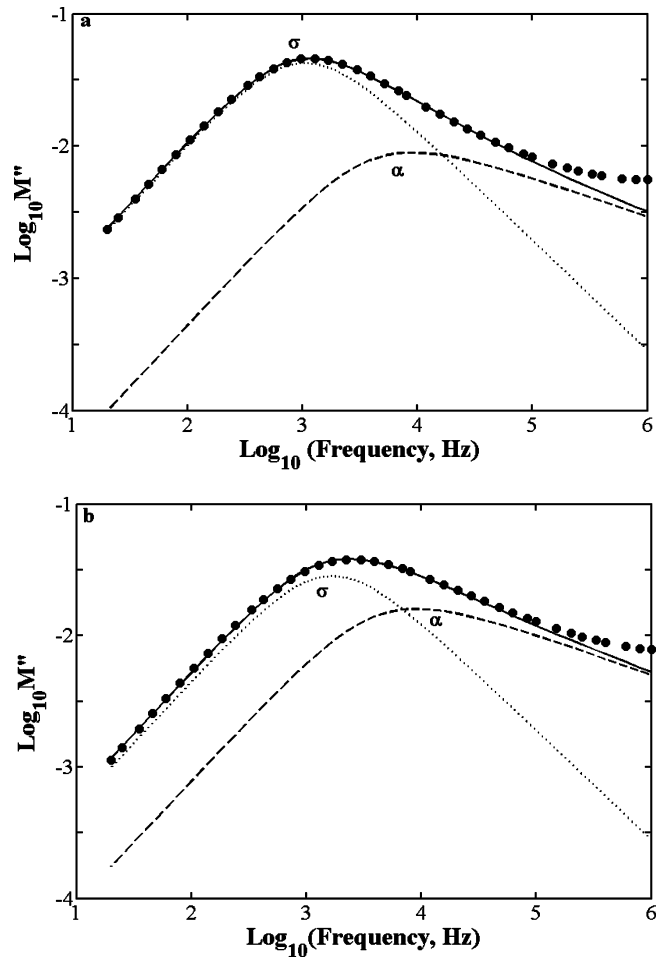

Figure 10. Fitting plot for dielectric loss modulus M'' vs frequency of silk fibroin protein at (a) 205 and (b) 214 °C after completion of crystallization at 214 °C, according to eq 3.

adjacent lines in the plot is ∼5 min. Figure 11a shows that the conductivity of the silk fibroin sample decreases as the isothermal crystallization proceeds. As more β-sheet crystal is formed, the transportation of free charge and ionic species becomes more difficult and, therefore, the decreasing rate of conductivity actually closely reflects the crystallization rate. The first 15−20 min during the crystallization process shows the largest decrease compared to later times, which means most of the β-sheet crystal is formed during that time period. Figure 11b shows that the dielectric permittivity ε' also decreases with crystallization time. ε' is related to the number density of effective dipole moments N and polarizability α as[43]

$$\varepsilon' - \varepsilon_0 = \alpha N = \langle \mu \rangle N/E \qquad (6)$$

where $\langle \mu \rangle$ is the average magnitude of one effective dipole moment in silk fibroin protein sample and E is the magnitude of the local electric field, at the position of the dipole moment. The decrease of ε' indicates a decrease of the product of the average dipole moment $\langle \mu \rangle$ and number density of dipole moments during the crystallization process, which will be elucidated in next section.

3.4. Relationship of Dielectric Properties to Silk Fibroin Structure. From the investigation of the isothermal crystallization process in silk with DRS, we observed that, during the crystallization, both the dielectric permittivity and electrical conductivity decrease. The α-relaxation, related to the

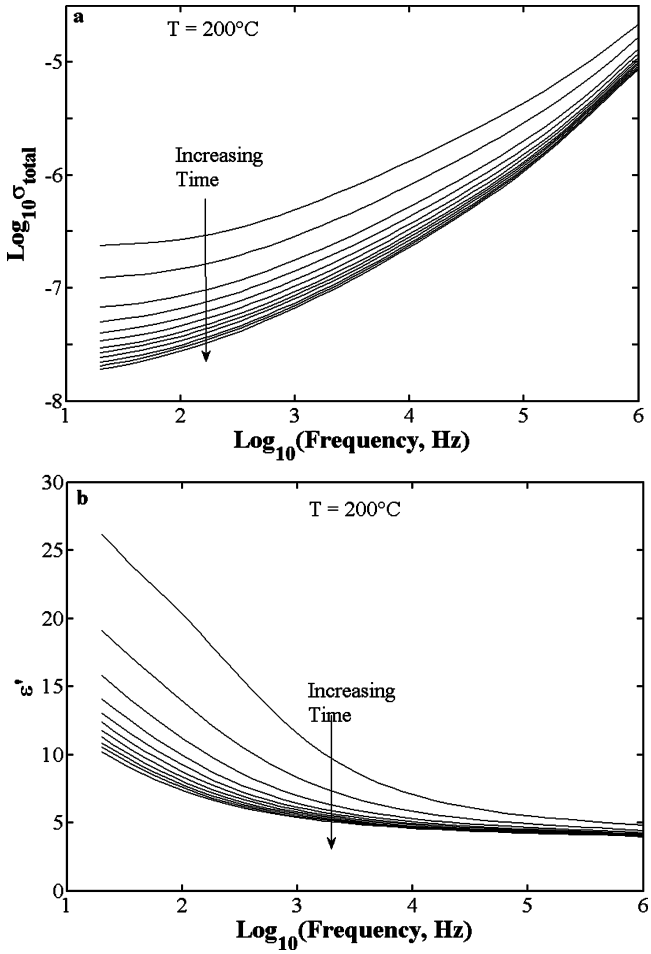

Figure 11. (a) Conductivity vs frequency during isothermal crystallization of silk fibroin protein at T_c = 200 °C. (b) Dielectric constant vs frequency during isothermal crystallization at T_c = 200 °C. The time difference between every two adjacent lines is around 5 min.

glass transition, became slower and weaker after the completion of crystallization. To understand how silk crystallization causes these effects, we introduce the structure of silk fibroin before furthering our discussion. *B. mori* silk fibroin is composed primarily of the amino acids, including glycine (G; ~42.9 mol %), alanine (A; ~30.0 mol %), serine (S; ~12.2 mol %), tyrosine (Y; ~4.8 mol %), and theronine (T; ~0.9 mol %).[11,44] Domains and subdomains in the structure of silk fibroin can be formed by these amino acids. A typical silk fibroin molecule consists of a heavy (H) chain domain (M_w ~ 350000 g/mol, with 5263 amino acids) and a light (L) chain domain (M_w ~ 25000 g/mol, with 262 amino acids), connected by a disulfide linkage. A structural model of silk fibroin protein was proposed by Ha et al.[4]

The H chain domain possesses an N-terminus and a C-terminus and is mainly composed of 12 repetitive domains whose typical composition are subdomains, including the repetitive amino acid sequences GAGAGS and GAGAGT. Ha et al.[4] showed that the GAGAGS segments are separated by 60 segments containing GY(GY~GY) sequences. The domains in the H chains are connected by 11 amorphous linkers, which include the α-helices, with 30 GT~GT amino acids in length each. Before crystallization, the 12 repetitive domains are fully amorphous and composed mainly of α-helices and random coils.[45] After being crystallized, the repetitive domains become transformed into antiparallel β-sheet crystals.[4] The light (L) chain domain is very small in size and does not have the repetitive domains found in the H chains. The L chains contain mostly random coils and do not crystallize.

Silk fibroin has been described as a block copolymer[14] combining crystallizable and noncrystallizable regions. Crystallizable regions mainly consist of the 12 repetitive domains in the H chains while noncrystallizable regions include random coils and amorphous linking groups. FTIR results from our previous work[12,13] showed that the intensity of the absorption bands from the α-helix/random coils *decrease*, while that of the β-sheet *increase* during the crystallization process. This is generally regarded as a proof that the α-helix/random coils are transformed into β-sheets gradually during the crystallization process. In support of this idea, Drummy et al.[45] studied thin film cast from the solution of *B. mori* silk in hexafluoroisopropyl alcohol (HFIP) solution by wide-angle X-ray diffraction during heating. They observed a conformational transition from the α-helical structure to the β-sheet structure. It was found that when the silk sample temperature is higher than 140 °C, the intramolecular hydrogen bonds in the α-helices are broken and the molecular chains can be stretched and transformed into β-strands.

Our data from the isothermal crystallization monitored by dielectric relaxation spectroscopy (DRS) leads to two main results: (1) dielectric constant ε′ decreases with the formation of silk fibroin crystal and (2) the α-relaxation, which is due to the glass transition of silk fibroin, diminishes after the formation of β-sheet crystals during the isothermal crystallization process. These two phenomena are the direct results of the transition from α-helices to β-sheets occurring within the crystallizable regions of silk fibroin. Figure 12 shows a general schematic representation of the arrangement of the dipole moments in the secondary structure of a protein. From Figure 12a, we can see the α-helix has a spiral structure and the alignment of peptide dipoles, C═O and N−H, parallel to the helical axis gives rise to a net dipole moment[46] along the axis of the α-helix. Each peptide unit has a dipole moment of ~3.5D so that a helix with 10 residues has a net dipole moment of 34D because 97% of peptide dipoles point along the direction of the helical axis.[47] Figure 12b,c shows the structure and dipole moment of the parallel and antiparallel β-sheets, respectively.[47] The parallel β-sheets have a net dipole moment along the β-strand direction because the peptide dipoles are oriented at an angle with the strand direction and do not cancel out. In contrast, in the antiparallel β-sheets, the peptide dipole moments are perpendicular to the strand direction and they all cancel out, giving no resultant dipole moment. The silk fibroin β-sheets are known to adopt the antiparallel conformation,[48−55] so the number density of dipole moments *decreases* during the crystallization process. From eq 6, the dielectric constant, ε′, decreases with the product of the average magnitude of an effective dipole moment $\langle\mu\rangle$ and the number density of the dipole moments. Because the transition from α-helices with a net dipole moment to antiparallel β-sheets without a net dipole moment reduces the number of effective dipole moments, the dielectric constant, ε′, decreases as crystallization proceeds.

Our results show that there are two discernible dielectric modulus relaxation peaks at the beginning of isothermal crystallization, which are recognized as the segmental α-relaxation (glass transition) and the conductivity relaxation. After crystallization is complete, the dielectric spectrum consists of conductivity relaxation and an α-relaxation with diminished strength and a slower rate. The reduction of the amount of effective dipole moments due to β-sheet crystallization is the reason for the decrease of the α-relaxation strength. As the

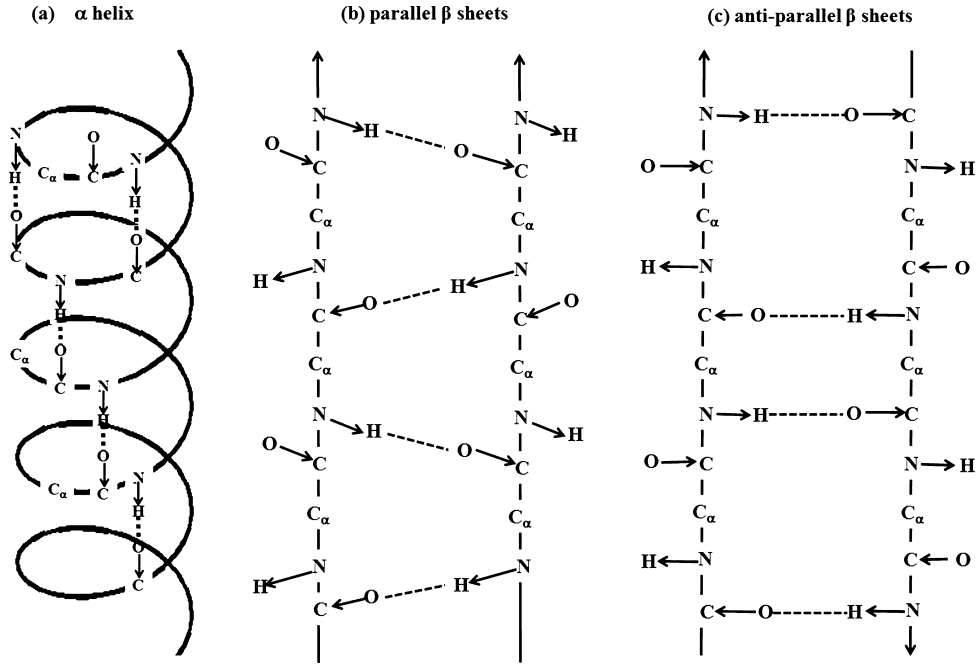

Figure 12. Molecular structure and dipole moment of silk fibroin protein: (a) α-helix; (b) parallel β-sheets; (c) antiparallel β-sheets. The arrow indicates the direction of the dipole moment. The dashed line represents the hydrogen bond. The α-helix shows a net dipole moment along the helix axis. The N→H and O→C bonds have different directions relative to the strand direction in the parallel and antiparallel β-sheets. In antiparallel β-sheets, these bonds are perpendicular to the β-strand direction with little or no resultant dipole moment. In parallel β-sheets, these bonds have an angle around 20° with the strand direction so there exists a net dipole moment along the β-strand direction. (b and c) Reproduced with permission from ref 47. Copyright 1981 *Nature*.

β-sheet crystal is formed, the transformation of the residual dipole moments from α-helices and random coils is restricted so the α-relaxation rate becomes slower. Both noncrystallizable amorphous parts, and the highly regular but not-yet-crystallized parts, are responsible for the segmental α-relaxation before the crystallization starts. As more and more amorphous segments in the highly regular crystallizable regions are transformed into β-sheet crystals, the α-relaxation strength contributed from this part is reduced. Noncrystallizable parts containing mostly random coils, α-helices, turns, and some side-chain groups, which possesses dipole moments are still dielectrically active during and after the crystallization process. Finally, the remaining noncrystallized parts within the crystallizable regions, as well as all of the noncrystallizable regions, are both responsible for the α-relaxation seen after the crystallization.

Real-time DRS has been used before to monitor the isothermal crystallization process of amorphous synthetic polymers.[56−61] In these works, several common phenomena during crystallization have been discussed, which indicate that the occurrence of crystallization in purely amorphous sample has several effects on the segmental α-relaxation, in the form of changes of the four dielectric parameters: (1) decrease of dielectric relaxation strength, $\Delta\varepsilon$; (2) shift of relaxation rate, f_{max}, to lower value indicating a slowing down of the α-relaxation; and, (3) change of the shape parameters, a and b. The α-dielectric relaxation strength is proportional to the amount of amorphous dipole moments; therefore, the onset of crystallization would decrease the α-relaxation strength. The emerging crystal lamellae could act as thermoreversible "crosslinks" to decrease the molecular mobility of the remaining amorphous polymer chains so the dielectric loss maximum f_{max} would shift to lower value. Developing crystalline domains produce restrictions on amorphous polymer chains, which are represented by the decrease of parameter $m = \beta$ (see eq 1), which stands for large scale motion as discussed earlier. The parameter $n = \beta\gamma$ (see eq 1) refers to smaller scale motions, which do not change much with crystallization. Real-time DRS of PET, PEN, and the copolymer P(HB-*co*-HV)[56−61] show similar changes in the dielectric parameters as described above.

In prior publications[56−61] on conventional synthetic polymers, primary and secondary relaxations are defined and discussed. During the isothermal crystallization process of conventional synthetic polymers, the primary relaxation occurs before the crystal lamellar stacks in the spherulites impinge upon each other. After spherulite impingement, secondary relaxation occurs within the interlamellar amorphous phase, and the relaxation rate f_{max} shows a characteristic discontinuous decrease occurring at around the crossover time between primary and secondary relaxation. In contrast to this behavior, silk fibroin exhibits a continuous decrease of f_{max}, which means that the α-relaxation is getting slower continuously from the beginning of the crystallization. Our recent scanning electron microscopy work[14] shows phase separation of crystallizable and noncrystallizable silk fibroin domains on a size scale from 100 to 200 nm and no formation of spherulites in silk fibroin protein. The phase separation results in a limitation of space available for crystallization, and therefore, a two-dimensional crystal growth mechanism is preferred in silk fibroin, as compared to the three-dimensional mechanism typically found in conventional synthetic polymers. The difference in the crystallization mechanism may be the reason why f_{max} shows different characteristic with crystallization time in silk fibroin compared to conventional synthetic polymers.

Conclusions

This study investigated the dielectric relaxation spectroscopy of both hydrated and dehydrated silk fibroin protein. When the temperature is below 0 °C, the β-relaxation, which occurs only in the hydrated sample, can be observed from −80 to −40 °C

in the temperature spectrum. This is related to the interaction of bound water molecules and C=O and N−H groups. The α′-relaxation peak in the temperature scan is attributed to the removal of bound water in silk fibroin. Both β- and α′-relaxation peaks are caused by the interaction between silk and the bound water molecules existing in the silk fibroin sample, and they disappear in the dehydrated sample. After bound water molecules are eliminated and the temperature is raised above the glass transition temperature T_g = 178 °C, DRS shows the coexistence of segmental α-relaxation and the DC conductivity relaxation process right before the onset of crystallization.

The α-relaxation is related to the α-helices and random coils possessing dipole moments located in the crystallizable and noncrystallizable regiosn of silk fibroin protein, which are both noncrystalline before crystallization starts. When crystallization occurs, the intramolecular hydrogen bonds in the α-helices are broken, and the helices are transformed into β-strands. Then, intermolecular hydrogen bonds are built up between β-strands and the antiparallel β-sheet crystalline structure, with no net dipole moment, is formed. Because the number density of effective dipole moments decreases as the crystallization occurs, the dielectric constant, ε′, decreases. The formation of the β-sheet crystal also results in the decrease of α-relaxation strength and rate, as deduced from the fitting process of the dielectric modulus. The conductivity of the silk fibroin sample is reduced with the growth of β-sheet crystals because the crystals serve as physical barriers to ion movement. We also compared the dielectric relaxation behavior of isothermal crystallization in conventional synthetic polymer to that of silk fibroin. Silk fibroin shows a different crystallization mechanism compared to conventional synthetic polymers, which can be explained by the formation of phase separated regions, due to the block-co-polymer nature of the silk fibroin, as introduced in our previous work.[14]

Acknowledgment. For support of this research, the authors thank the National Science Foundation under DMR-0602473 and CBET-0828028.

References and Notes

(1) Vepari, C.; Kaplan, D. L. *Prog. Polym. Sci.* **2007**, *8—9*, 991–1007.
(2) Zhao, C. H.; Asakura, T. *Prog. Nucl. Magn. Reson. Spectrosc.* **2001**, *4*, 301–352.
(3) Hakimi, O.; Knight, D. P.; Vollrath, F.; Vadgama, P. *Composites, Part B* **2007**, *3*, 324–337.
(4) Ha, S. W.; Gracz, H. S.; Tonelli, A. E.; Hudson, S. M. *Biomacromolecules* **2005**, *5*, 2563–2569.
(5) Putthanarat, S.; Stribeck, N.; Fossey, S. A.; Eby, R. K.; Adams, W. W. *Polymer* **2000**, *21*, 7735–7747.
(6) Knight, D. P.; Vollrath, F. *Philos. Trans. R. Soc., B* **2002**, *1418*, 155–163.
(7) Altman, G. H.; Diaz, F.; Jakuba, C.; Calabro, T.; Horan, R. L.; Chen, J. S.; Lu, H.; Richmond, J.; Kaplan, D. L. *Biomaterials* **2003**, *3*, 401–416.
(8) Foo, C. W. P.; Kaplan, D. L. *Adv. Drug Delivery Rev.* **2002**, *8*, 1131–1143.
(9) *Silk Polymers - Materials Science and Biotechnology*; Kaplan, D., Adams, W. W., Farmer, B., Viney, C., Eds.; ACS Symposium Series 544; American Chemical Society: Washington, DC, 1994; pp 2−16.
(10) Sashina, E. S.; Bochek, A. M.; Novoselov, N. P.; Kirichenko, D. A. *Russ. J. Appl. Chem.* **2006**, *6*, 869–876.
(11) McGrath, K., Kaplan, D., Eds. *Protein-Based Materials*; Birkhauser Press: Boston, 1996.
(12) Hu, X.; Kaplan, D.; Cebe, P. *Macromolecules* **2006**, *18*, 6161–6170.
(13) Hu, X.; Kaplan, D.; Cebe, P. *Macromolecules* **2008**, *11*, 3939–3948.
(14) Hu, X.; Lu, Q.; Kaplan, D. L.; Cebe, P. *Macromolecules* **2009**, *6*, 2079–2087.
(15) Zhang, X.; Reagan, M. R.; Kaplan, D. L. *Adv. Drug Delivery Rev.* **2009**, *12*, 988–1006.
(16) Yu, L.; Cebe, P. *Polymer* **2009**, *9*, 2133–2141.
(17) Sun, M. Y.; Pejanovic, S.; Mijovic, J. *Macromolecules* **2005**, *23*, 9854–9864.
(18) Mijovic, J.; Bian, Y.; Gross, R. A.; Chen, B. *Macromolecules* **2005**, *26*, 10812–10819.
(19) Magoshi, J.; Magoshi, Y. *J. Polym. Sci., Part B: Polym. Phys.* **1975**, *7*, 1347–1351.
(20) Um, I. C.; Kim, T. H.; Kweon, H. Y.; Ki, C. S.; Park, Y. H. *Macromol. Res.* **2009**, *10*, 785–790.
(21) Motta, A.; Fambri, L.; Migliaresi, C. *Macromol. Chem. Phys.* **2002**, *203*, 1658–1665.
(22) Asakura, T.; Kaplan, D. L. *Silk Production and Processing*; Academic Press: New York, 1994; Vol. 4, p1.
(23) Zhou, C. Z.; Confalonieri, F.; Medina, N.; Zivanovic, Y.; Esnault, C.; Yang, T.; Jacquet, M.; Janin, J.; Duguet, M.; Perasso, R.; Li, Z. G. *Nucleic Acids Res.* **2000**, *28*, 2413–2419.
(24) Gulrajani, M. L. *Rev. Prog. Color.* **1992**, *22*, 79–89.
(25) Ishida, M.; Asakura, T.; Yokoi, M.; Saito, H. *Macromolecules* **1990**, *1*, 88–94.
(26) Walters, R. H.; Hougen, O. A. *Text. Res. J.* **1934**, *5*, 92–104.
(27) Nogales, A.; Ezquerra, T. A.; Rueda, D. R.; Martinez, F.; Retuert, J. *Colloid Polym. Sci.* **1997**, *275*, 419–425.
(28) Hu, X.; Kaplan, D.; Cebe, P. *Thermochim. Acta* **2007**, *461*, 137–144.
(29) Laredo, E.; Hernandez, M. C. *J. Polym. Sci., Part B: Polym. Phys.* **1997**, *17*, 2879–2888.
(30) Frank, B.; Frubing, P.; Pissis, P. *J. Polym. Sci., Part B: Polym. Phys.* **1996**, *11*, 1853–1860.
(31) Havrilia, S.; Negami, S. *Polymer* **1967**, *4*, 161.
(32) Yu, L.; Cebe, P. *J. Polym. Sci., Part B: Polym. Phys.* **2009**, *24*, 2520–2532.
(33) Kremer, F.; Schonhals, A. *Broadband Dielectric Spectroscopy*; Springer: Berlin, Germany, 2002; p 71.
(34) Bello, A.; Laredo, E.; Grimau, M. *J. Non-Cryst. Solids* **2007**, *47—51*, 4283–4287.
(35) Lee, H.; Pejanovic, S.; Mondragon, I.; Mijovic, J. *Polymer* **2007**, *25*, 7345–7355.
(36) Pissis, P.; Kyritsis, A. *Solid State Ionics* **1997**, *1—4*, 105–113.
(37) Pissis, P.; Kyritsis, A.; Georgoussis, G.; Shilov, V. V.; Shevchenko, V. V. *Solid State Ionics* **2000**, 255–260.
(38) El Moznine, R.; Smith, G.; Polygalov, E.; Suherman, P. M.; Broadhead, J. *J. Phys. D: Appl. Phys.* **2003**, *4*, 330–335.
(39) Mohomed, K.; Gerasimov, T. G.; Moussy, F.; Harmon, J. P. *Polymer* **2005**, *11*, 3847–3855.
(40) Ambrus, J. H.; Macedo, P. B.; Moynihan, C. T. *J. Phys. Chem.* **1972**, *22*, 3287.
(41) Johari, G. P.; Pathmanathan, K. *Phys. Chem. Glasses* **1988**, *6*, 219–224.
(42) Macedo, P. B.; Moynihan, C. T.; Bose, R. *Phys. Chem. Glasses* **1972**, *6*, 171–179.
(43) Kao;K. C. *Dielectric Phenomena in Solids: With Emphasis on Physical Concepts of Electronic Processes*; Elsevier Academic Press: San Diego, CA, 2004; p 56.
(44) Pyda, M.; Hu, X.; Cebe, P. *Macromolecules* **2008**, *13*, 4786–4793.
(45) Drummy, L. F.; Phillips, D. M.; Stone, M. O.; Farmer, B. L.; Naik, R. R. *Biomacromolecules* **2005**, *6*, 3328–3333.
(46) Wada, A. *Adv. Biophys.* **1976**, 1–63.
(47) Hol, W. G. J.; Halie, L. M.; Sander, C. *Nature* **1981**, *5841*, 532–536.
(48) Chen, X.; Knight, D. P.; Shao, Z. Z.; Vollrath, F. *Polymer* **2001**, *25*, 9969–9974.
(49) Chen, X.; Shao, Z. Z.; Marinkovic, N. S.; Miller, L. M.; Zhou, P.; Chance, M. R. *Biophys. Chem.* **2001**, *1*, 25–34.
(50) Tretinnikov, O. N.; Tamada, Y. *Langmuir* **2001**, *23*, 7406–7413.
(51) Taddei, P.; Monti, P. *Biopolymers* **2005**, *5*, 249–258.
(52) Wilson, D.; Valluzzi, R.; Kaplan, D. *Biophys. J.* **2000**, *5*, 2690–2701.
(53) Marsh, R. E.; Corey, R. B.; Pauling, L. *Biochem. Biophys. Acta.* **1955**, *16*, 1.
(54) Fraser, R. D.; MacRae, T. P.; Stewart, F. H. *J. Mol. Biol.* **1966**, *19*, 580–589.
(55) Lotz, B.; Brack, A.; Spach, G. *J. Mol. Biol.* **1974**, *87*, 193–202.
(56) Alvarez, C.; Sics, I.; Nogales, A.; Denchev, Z.; Funari, S. S.; Ezquerra, T. A. *Polymer* **2003**, *45*, 3953–3959.
(57) Ezquerra, T. A.; Sics, I.; Nogales, A.; Denchev, Z.; Balta-Calleja, F. J. *Europhys. Lett.* **2002**, *3*, 417–422.
(58) Sics, I.; Ezquerra, T. A.; Nogales, A.; Balta-Calleja, F. J.; Kalnins, M.; Tupureina, V. *Biomacromolecules* **2001**, *2*, 581–587.
(59) Sics, I.; Ezquerra, T. A.; Nogales, A.; Denchev, Z.; Alvarez, C.; Funari, S. S. *Polymer* **2003**, *4*, 1045–1049.
(60) Verma, R.; Marand, H.; Hsiao, B. *Macromolecules* **1996**, *24*, 7767–7775.
(61) Huo, P. T.; Cebe, P. *J. Polym. Sci., Part B: Polym. Phys.* **1992**, *3*, 239–250.

BM1008316